# All-electrochem-active silicon anode enabled by spontaneous Li-Si alloying for ultra-high performance solid-state batteries

*Zhiyong Zhang [1], Zhefei Sun [2], Xiang Han [3], Yan Liu [4], Shanpeng Pei [1,5], Yahui Li [1], Linshan Luo [1], Pengfei Su [1], Chaofei Lan [1], Ziqi Zhang [6], Shaowen Xu [1], Shengshi Guo [1], Wei Huang [1]*, Songyan Chen [1]*, and Ming-Sheng Wang [2]**

[1] Department of Physics, Collaborative Innovation Center for Optoelectronic Semiconductors and Efficient Devices, Key Laboratory of Low Dimensional Condensed Matter Physics (Department of Education of Fujian Province), Jiujiang Research Institute, Xiamen University, Xiamen 361005, China

[2] State Key Lab of Physical Chemistry of Solid Surfaces, College of Materials, Xiamen University, Xiamen 361005, China

[3] College of Materials Science and Engineering, Nanjing Forestry University, Nanjing 210037, China

[4] School of Semiconductor Science and Technology South China Normal University, Foshan 528225, China

[5] Shandong Electric Power Engineering consulting Institute Corporation, Jinan 250031, China

[6] Science and Technology on Analog Integrated Circuit Laboratory, Chongqing 400000, China

Corresponding author: sychen@xmu.edu.cn, mswang@xmu.edu.cn, weihuang@xmu.edu.cn

Keywords: solid-state silicon anode, $Li_{21}Si_5$ alloy, spontaneous reaction, all-electrochem-active, ultra-high ICE

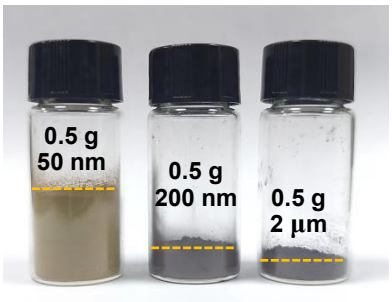


Supplementary Figure 1. Comparison of the stacked densities for various Si powders with different particle sizes.

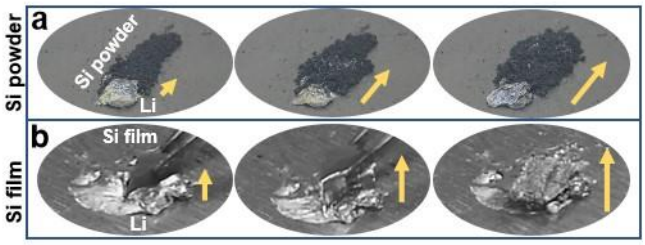


Supplementary Figure 2. Effect of Si powder's stacked density on direction of the spontaneous reaction. (a) Photographs of 1 g Si powder as a flat layer when reacting with molten Li. (b) Photographs of a standing of 20 mm×20 mm×3 mm film when reacting with molten Li.

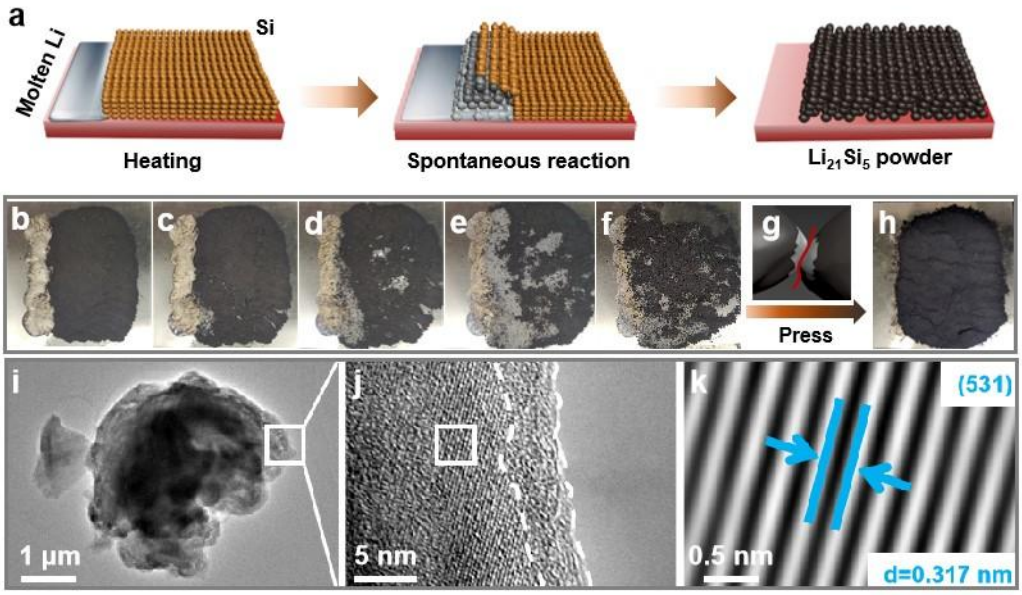


Supplementary Figure 3. Fragmentation process and structural characterization of the $Li_{21}Si_5$ particles. (a-h) The $Li_{21}Si_5$ synthesis process. (i) TEM image of the $Li_{21}Si_5$ particle. (j) an enlargement of Supplementary Figure 3i. (k) Fourier inverse transformation image of the boxed area in Supplementary Figure 3j.

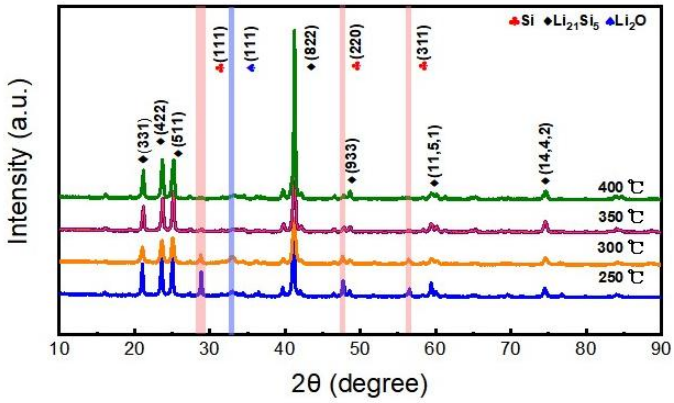


Supplementary Figure 4. XRD patterns of the synthesized $Li_{21}Si_5$ powder from 5 g Si powder with different reaction temperatures (250, 300, 350, and 400 ℃) in 60 s.

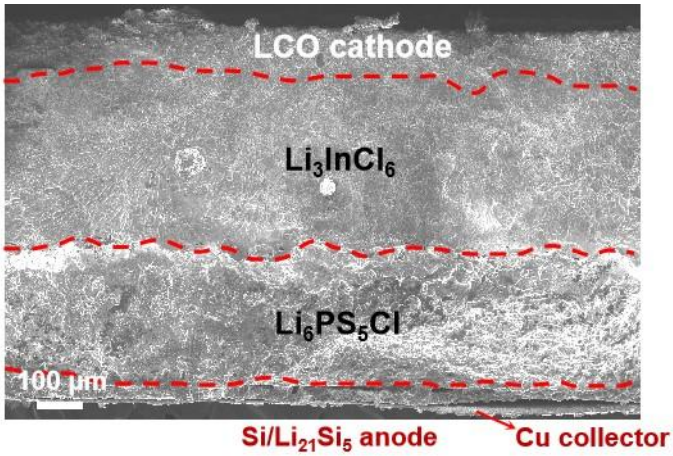


Supplementary Figure 5. Cross-section SEM of $Si/Li_{21}Si_5$-ASSB.

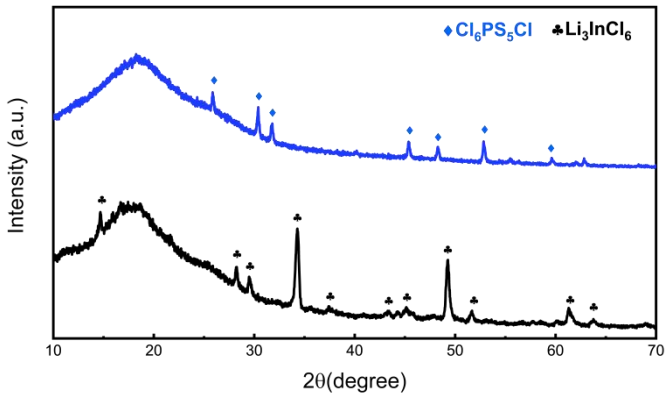


Supplementary Figure 6. XRD pattern of $Li_3InCl_6$ and $Li_6PS_5Cl$.

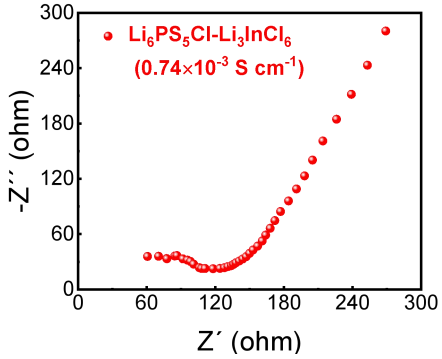


Supplementary Figure 7. Ionic conductivity of composite bilayer solid electrolyte.

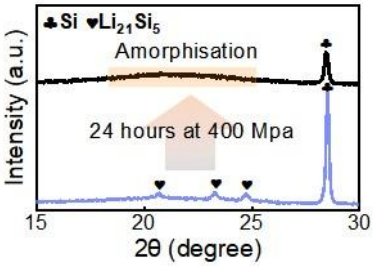


Supplementary Figure 8. XRD pattern of $Si/Li_{21}Si_5$ anode after cold press at 400 Mpa.

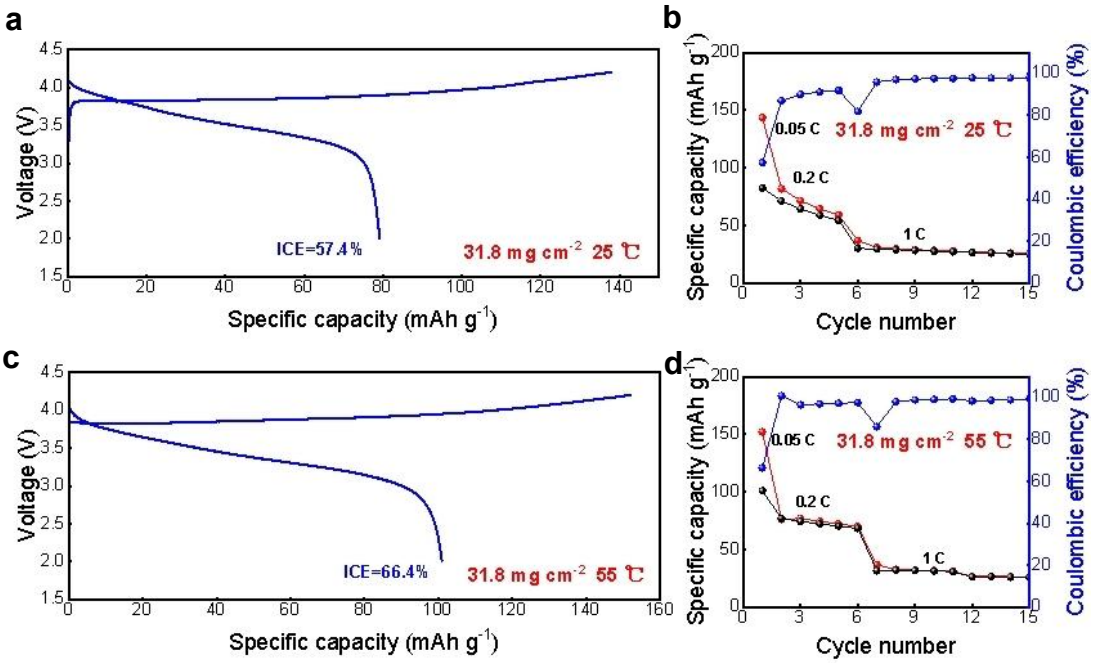


Supplementary Figure 9. The cycle performance of pure Si-ASSBs. a and b were first charge-discharge cycle and different rate cycle curves of Si-ASSBs at room temperature. c and d were first charge-discharge cycle and different rate cycle curves of at high temperature.

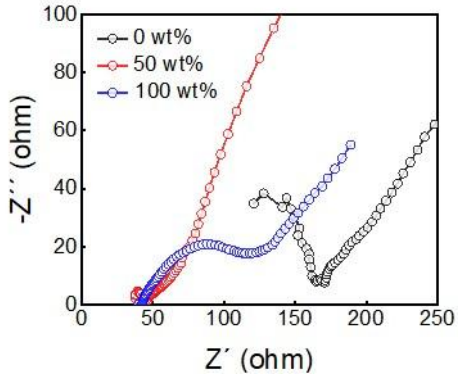


Supplementary Figure 10. EIS spectra of Si/$Li_{21}Si_5$-ASSBs with 0 wt%, 50 wt% and 100 wt% of $Li_{21}Si_5$ powder.

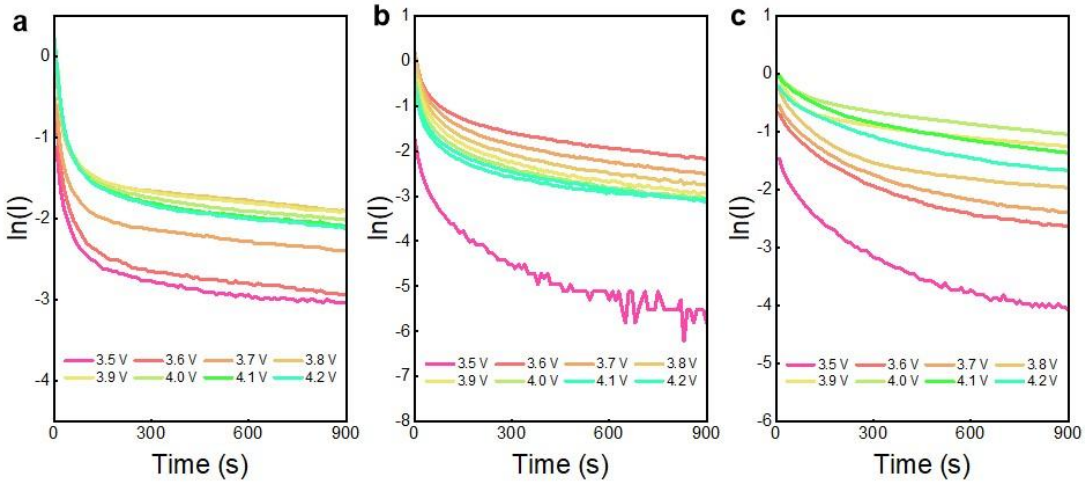


Supplementary Figure 11. PITT curves of LFP | SE | Si (a), LFP | SE | Si/$Li_{21}Si_5$ (b), and LFP | SE | $Li_{21}Si_5$ (c). The PITT tests were operated at 55 ℃.

Supplementary Table 1 | The dates of face capacity and ICE in the published literature.

| Reference | Capacity (mAh $cm^{-2}$) | ICE (%) | Cathode | Journals | Year |
|---|---|---|---|---|---|
| Ref.23 | 0.05 | 71.00 | LFP | ACS Appl. Mater. Interfaces | 2018 |
| Ref.24 | 3 | 87.50 | LZO@NCM | Adv. Energy Mater. | 2020 |
| Ref.14 | 3 | 77.92 | B@NCM | Science | 2021 |
| | 4.5 | 80.35 | | | |
| | 11.1 | 84.73 | | | |
| Ref.25 | 2.5 | 67.57 | LCO | Adv. Energy Mater. | 2022 |
| Ref.26 | 1.9 | 81.52 | $Li_2SiO_x$@S-NMC | Adv. Mater. | 2022 |
| Ref.27 | 2 | 74.70 | NCM | Energy Environ. Sci. | 2023 |
| Ref.13 | 3.3 | 74.00 | $Li_2SiO_x$@S-NMC | Adv. Energy Mater. | 2023 |
| Ref.15 | 1.4 | 80.00 | LATP@NCM | Nat. Energy | 2023 |
| | 5.7 | 83.30 | | | |
| | 10.7 | 82.79 | | | |
| | 17.0 | 82.93 | | | |
| | 1.2 | 90.00 | LCO | | |
| Ref.28 | 2.3 | 84.80 | LCO | Adv. Energy Mater. | 2023 |
| Ref.29 | 1.5 | 71.60 | $LiNbO_3$@NCM | Small | 2023 |
| This work | 3.5 | 97.19 | LCO | | 2023 |
| | 8.9 | 96.90 | | | |
| | 17.9 | 96.85 | | | |

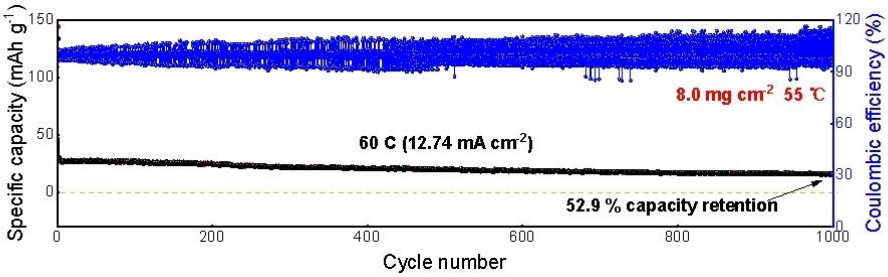


Supplementary Figure 12. The long cycles of ultra-high rate of 60 C.